JOURNAL OF APPLIED ELECTROCHEMISTRY 16 (1986) 605–614

Electrodissolution kinetics of an Fe–Ni alloy in acidic chloride media of 1.0 M ionic strength

N. L. NGUYEN, KEN NOBE*

Department of Chemical Engineering, University of California, Los Angeles, California 90024, USA

Received 6 February 1985; revised 10 September 1985

Anodic dissolution of an Fe–5Ni alloy in deoxygenated acidic chloride solutions of 1.0 M ionic strength has been studied. Steady state partial current densities of the iron and nickel components were obtained by atomic absorption spectrophotometry analysis of the solutions. Alloy and component electrodissolution rates show two anodic Tafel regions indicating simultaneous parallel reactions as reported previously for pure iron. Anodic Tafel slopes of 0.075 and 0.04 V dec^{-1} were obtained in the lower (A) and higher (B) polarization regions, respectively. The kinetic results for the alloy are consistent with the Cl^- accelerated mechanism in Region (A) and the Bockris or OH^- accelerated mechanism in Region (B) for both iron and nickel components as proposed previously for pure iron.

1. Introduction

Anodic dissolution of iron and nickel in the absence and presence of chloride ions has been studied by a number of investigators (e.g., [1–18]). Although a complete understanding of the kinetics and mechanisms of iron and nickel electrodissolution has not yet been achieved, nevertheless much basic information has been gained during the past twenty years. On the other hand, few fundamental studies of the more complex systems of Fe–Ni alloys have been reported. For the pure iron system it has been shown that the addition of chloride ions to acidic media signifiantly affects the kinetics and mechanism of Fe electrodissolution [10, 19]. There is also evidence that there are similar effects in nickel electrodissolution [18]. For this reason, it would be of interest to examine the chloride effect on Fe–Ni alloys.

There have been a few anodic dissolution studies of Fe–Ni alloys in H_2SO_4 [20–22] and in acidic chloride media [23]. However, the kinetic information obtained in these studies was rather limited and precluded consideration of alloy electrodissolution mechanisms. This paper reports initial electrodissolution kinetic studies of a Fe–5 wt % Ni alloy in acidic chloride solutions of constant 1 M ionic strength. The results are compared with those obtained previously for pure iron [9] and pure nickel [18].

2. Experimental details

Electrodes were prepared from 0.95 cm diameter rod of Fe–5.32 wt % (5.08 g atom %) Ni alloy (Magnetics Co.). The rod was turned on a lathe to cross-sectional areas of 0.625 and 0.10 cm^2. The electrodes were polished with alumina paper (grit no. 240, 400 and 600), and then degreased with hot benzene in a Soxhlet column for 4 h, annealed under vacuum (10^{-5} torr) at 510° C for 1 h, allowed to cool slowly to room temperature and stored in a dessicator until used.

* To whom correspondence should be addressed.

0021–891X/86 $03.00 + .12

Descriptions of the rotaing disc electrode unit and the three-electrode electrochemical cell have been given previously [24]. A PAR potentiostat (model 173) with log current converter unit (model 376) and a PAR universal programmer (model 175) provided potential control. A Perkin–Elmer atomic absorption spectrophotometer was used for solution analyses.

Deionized water, which was then double distilled, and analytical reagent grade chemicals were used to prepare the electrolyte solutions, 1 M (NaCl + HCl) and 1 M (HCl + $HClO_4$). For solutions containing perchlorate ions, a fibre junction salt bridge filled with 4.2 M NaCl was inserted between the reference electrode (saturated calomel electrode) and the electrolyte. The solutions were deoxygenated with prepurified nitrogen gas (Liquid Carbonics) for 15 h before immersion of the rotating disc electrode. Before passage through the solution, the prepurified nitrogen gas was first passed through a heated Vycor glass column containing copper filings at 450° C.

After immersion of a fresh electrode in the solution, steady state corrosion potentials were usually attained within 1–2 h; polarization was then initiated. Potential steps were applied from the corrosion potential (in increments of 25 or 50 mV) for a normal polarization time of 30 min (steady state polarization was usually achieved within a few minutes). At the end of each potential step the electrode was returned to the corrosion potential (usually attained within 3–5 min). Solution samples were then taken for atomic absorption spectrophotometry analysis. At low rates of electrodissolution, polarization times were increased to 3–5 h since changes in metal ion concentrations in the solution at the normal 30 min polarization time were too small for accurate determinations. A fresh electrode was used for each polarization run.

All potentials reported in this paper have been corrected for *IR* drops and liquid junction potentials.

3. Results

The corrosion potentials of the rotating alloy discs in acidic chloride solutions were found to be independent of rotation rate (rotation rates were varied up to 5000 r.p.m.). The dependence of the corrosion potential on pH is shown in Fig. 1 where

$$\frac{\partial E_{\text{corr}}}{\partial \text{pH}} = -0.05\ \text{V pH}^{-1} \tag{1}$$

Its dependence on chloride ions is shown in Fig. 2 where

$$\frac{\partial E_{\text{corr}}}{\partial \log [\text{Cl}^-]} = -0.05\ \text{V dec}^{-1} \tag{2}$$

The corrosion currents were determined by anodic Tafel extrapolation and polarization resistance measurements. The dependence of the corrosion current on pH,

$$\frac{\partial \log i^{\text{a}}_{\text{corr}}}{\partial \text{pH}} = -0.2 \tag{3}$$

and on chloride ions,

$$\frac{\partial \log i^{\text{a}}_{\text{corr}}}{\partial \log [\text{Cl}^-]} = 0.2 \tag{4}$$

are also shown in Figs 1 and 2, respectively. The superscript 'a' refers to the alloy.

Equation 1 is in good agreement with that reported by Economy *et al.* [21] for Fe–5 Ni in H_2SO_4. Equation 3 is one-half the value reported by Chin [9] for iron in acidic chloride solutions; he also reported $\delta \log i_{\text{corr}}/\delta \log [\text{Cl}^-] = 0.3$ for iron compared to a value of 0.2 for the alloy (Equation 4).

Fig. 3 shows the dependence of anodic dissolution of the alloy in acidic chloride solutions on pH.

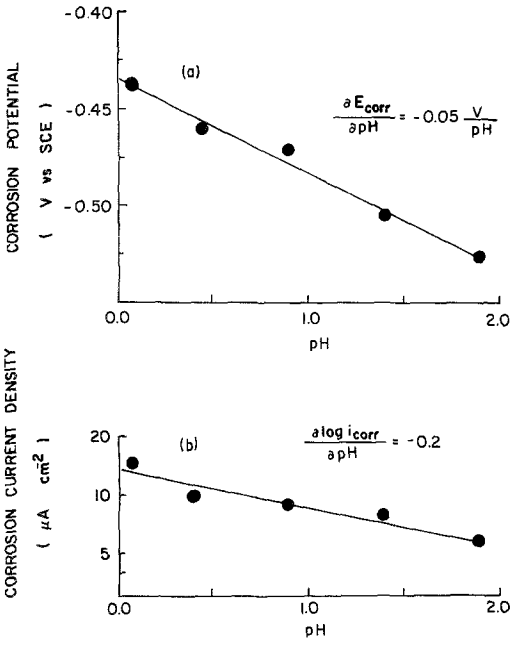

Fig. 1. The dependence of (a) corrosion potential and (b) corrosion current density on pH for Fe–5Ni alloy in 1 M (HCl + NaCl).

Two anodic polarization regions, as distinguished by different Tafel slopes, are discerned. At lower anodic polarization,

$$b_a = \left(\frac{\partial E}{\partial \log i^a}\right)_{pH} = 0.075\,\mathrm{V\,dec^{-1}} \tag{5}$$

while at higher anodic polarization,

$$b_a = \left(\frac{\partial E}{\partial \log i^a}\right)_{pH} = 0.040\,\mathrm{V\,dec^{-1}} \tag{6}$$

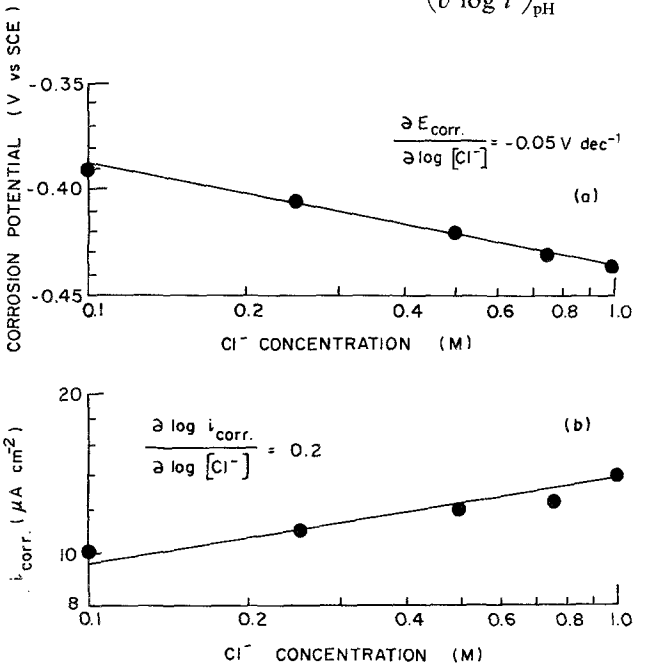

Fig. 2. The dependence of corrosion potential and corrosion current density on Cl^- concentration for Fe–5Ni alloy in 1 M (HCl + $HClO_4$).

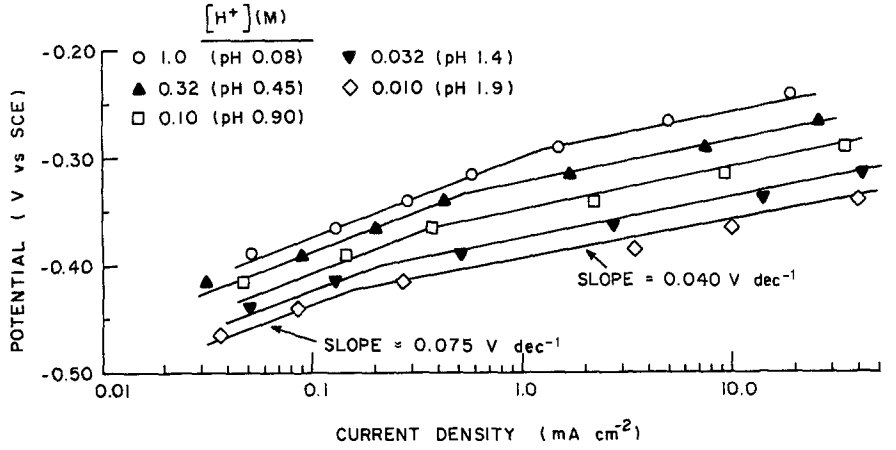

Fig. 3. Effect of pH on anodic polarization of Fe–5Ni alloy in 1 M (HCl + NaCl).

In both polarization regions, the rate of anodic dissolution increases with increase in pH. The pH reaction order plots for alloy electrodissolution are given in Fig. 4. In the lower anodic polarization region, the pH reaction order is 0.5, that is,

$$\left(\frac{\partial \log i^{a}_{Fe\text{-}5Ni}}{\partial \text{ pH}}\right)_{E_a} = 0.5 \tag{7}$$

On the other hand, in the higher anodic polarization region,

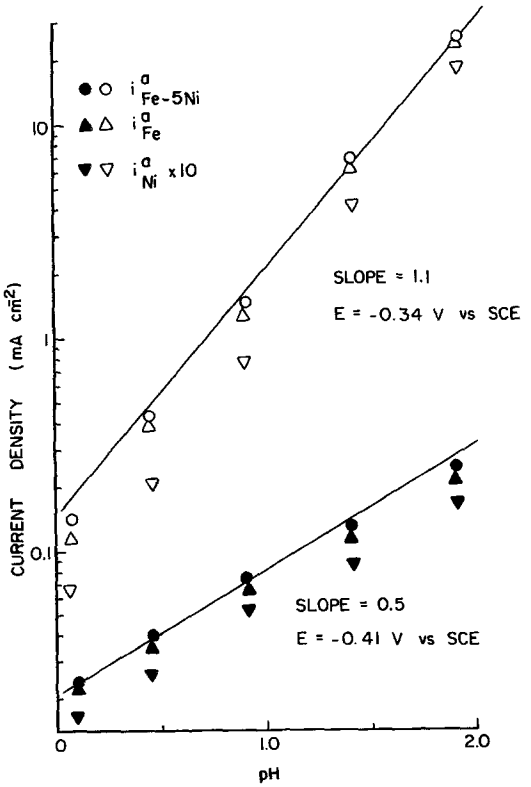

Fig. 4. pH reaction order plots for Fe–5Ni alloy electrodissolution in 1 M (HCl + NaCl).

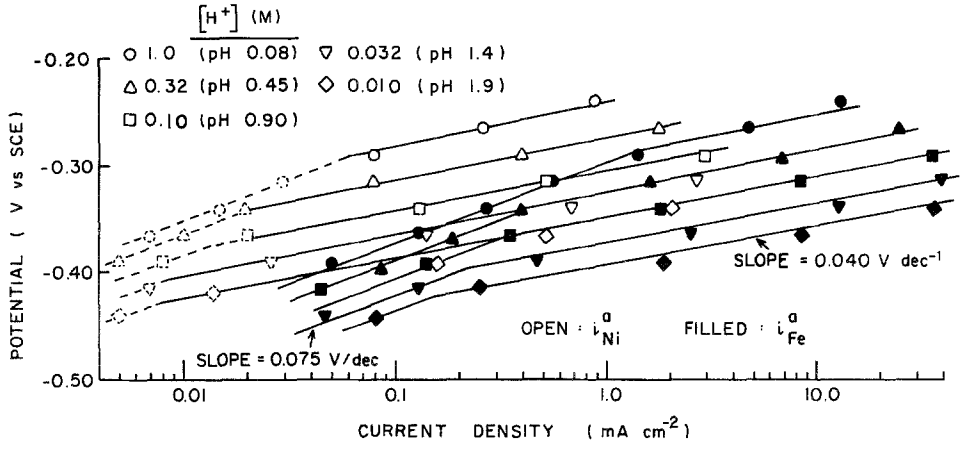

Fig. 5. Effect of pH on electrodissolution rates of iron and nickel components in 1 M (HCl + NaCl).

$$\left(\frac{\partial \log i^{a}_{Fe\text{-}5Ni}}{\partial pH}\right)_{E_a} = 1.1 \tag{8}$$

The anodic polarization behaviour, the anodic Tafel slopes and the pH reaction orders are the same as those observed by Kuo and Nobe for pure iron [10].

Fig. 5 shows the results of the atomic absorption solution analyses for both iron and nickel (the dashed points represent data for nickel calculated by difference of $i^{a}_{Fe\text{-}5Ni}$ and iron analyses). The anodic polarization plots of these results for the iron and nickel components also show the two polarization regions as the alloy (Fig. 3). The latter gives the alloy electrodissolution rate while Fig. 5 gives the electrodissolution rate of the iron and nickel components separately. Fig. 5 indicates that the anodic polarization behaviour of the iron and nickel components are similar, even though the nickel electrodissolution rate is substantially lower than iron. For both iron and nickel components anodic Tafel slopes in the lower and higher polarization regions are represented by Equations 5 and 6, respectively.

The pH reaction order plots for electrodissolution of the iron and nickel components are also shown in Fig. 4. It is seen that the reaction orders for the iron and nickel components are the same as the alloy in both polarization regions. That is, in the lower polarization region,

$$\left(\frac{\partial \log i^{a}_{Fe\text{-}5Ni}}{\partial pH}\right)_{E_a} = \left(\frac{\partial \log i^{a}_{Fe}}{\partial pH}\right)_{E_a} = \left(\frac{\partial \log i^{a}_{Ni}}{\partial pH}\right)_{E_a} = 0.5 \tag{9}$$

and the higher polarization region,

$$\left(\frac{\partial \log i^{a}_{Fe\text{-}Ni}}{\partial pH}\right)_{E_a} = \left(\frac{\partial \log i^{a}_{Fe}}{\partial pH}\right)_{E_a} = \left(\frac{\partial \log i^{a}_{Ni}}{\partial pH}\right)_{E_a} = 1.1 \tag{10}$$

The dependence of anodic dissolution of the alloy on chloride ions is shown in Fig. 6. Two anodic polarization regions are again observed with Tafel slopes,

$$b_a = \left(\frac{\partial E}{\partial \log i^{a}}\right)_{[Cl^-]} = 0.075\,V\,dec^{-1} \tag{11}$$

at lower polarization, and

$$b_a = \left(\frac{\partial E}{\partial \log i^{a}}\right)_{[Cl^-]} = 0.040\,V\,dec^{-1} \tag{12}$$

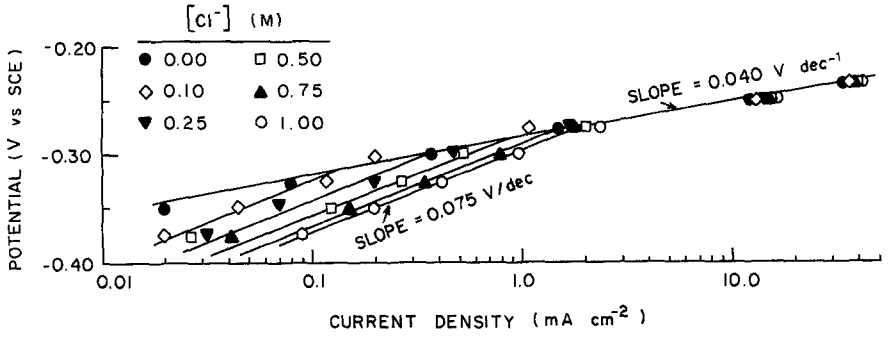

Fig. 6. Effect of Cl^- on anodic polarization of Fe–5Ni alloy in 1 M ($HCl + HClO_4$).

at higher polarization. However, in contrast to the higher polarization region of the alloy for the pH dependent behaviour (Fig. 3), no chloride concentration dependence is observed (Fig. 6), that is,

$$\left(\frac{\partial \log i^{a}_{Fe\text{-}5Ni}}{\partial \log [Cl^-]}\right)_{E_a} = 0 \tag{13}$$

On the other hand, at lower polarization, anodic dissolution rates of the alloy increase with increasing chloride concentration. The chloride reaction order plot given in Fig. 7 shows that

$$\left(\frac{\partial \log i^{a}_{Fe\text{-}5Ni}}{\partial \log [Cl^-]}\right)_{E_a} = 0.5 \tag{14}$$

for the lower polarization region. It should be noted that in the complete absense of chloride ions only a single Tafel line with slope of 0.040 V dec^{-1} is obtained (Fig. 6). This result is in accord with results obtained for pure iron [10, 19].

A similar polarization behaviour, as obtained from the atomic absorption measurements, are observed for the iron and nickel components (Fig. 8). In the higher polarization region ($b_a = 0.040\,V\,dec^{-1}$),

$$\left(\frac{\partial \log i^{a}_{Fe}}{\partial \log [Cl^-]}\right)_{E_a} = \left(\frac{\partial \log i^{a}_{Ni}}{\partial \log [Cl^-]}\right)_{E_a} = 0 \tag{15}$$

At lower anodic polarization ($b_a = 0.075\,V\,dec^{-1}$), as shown by the reaction order plots of Fig. 7 for both iron and nickel component electrodissolution,

$$\left(\frac{\partial \log i^{a}_{Fe}}{\partial \log [Cl^-]}\right)_{E_a} = \left(\frac{\partial \log i^{a}_{Ni}}{\partial \log [Cl^-]}\right)_{E_a} = 0.5 \tag{16}$$

The results in Figs 7 and 8 show that the electrodissolution rate of the nickel component is significantly lower than the rate of the iron component.

The atomic absorption measurements indicate that, except in the vicinity of the corrosion potential, the electrodissolution of the Fe–5Ni alloy is non-selective (the g atom ratio of nickel to iron for the bulk alloy is 0.053). Pitting was observed in the higher polarization region at higher acidic chloride concentrations.

4. Discussion

The empirical rate expressions for the electrodissolution of both iron and nickel components in the Fe–5Ni alloy are as follows:

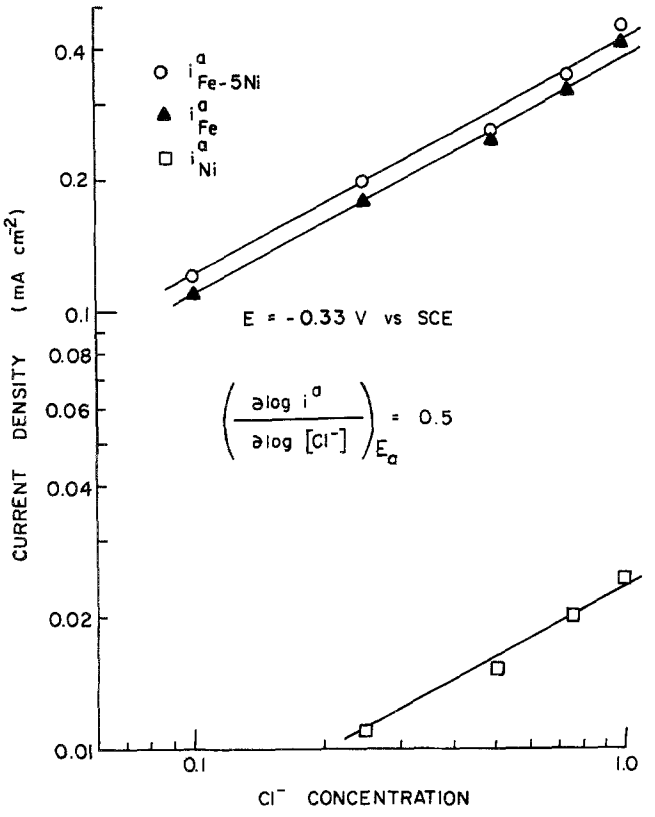

Fig. 7. Cl^- reaction order plots for Fe–5Ni alloy electrodissolution in 1 M ($HCl + HClO_4$).

$$i_j^a(A) = 2Fk_j^a(A)[Cl^-]^{0.5}[H^+]^{-0.5} \exp\left(\frac{4FE}{5RT}\right) \tag{17}$$

for the lower anodic polarization Region (A), and

$$i_j^a(B) = 2Fk_j^a(B)[H^+]^{-1.1} \exp\left(\frac{3FE}{2RT}\right) \tag{18}$$

for the higher anodic polarization Region (B). Subscript j represents either the iron or nickel component.

The kinetic Equations 17 and 18, which apply to the electrodissolution of both iron and nickel components, can be interpreted as representing two coupled parallel reactions, the Cl^- accelerated [9] and the OH^- accelerated [2] mechanisms; the concept of the two parallel reactions had been previously proposed for pure iron [9, 10] and pure nickel [18]. Bech-Nielsen [25–27] has provided experimental results and analyses of parallel reactions in anodic dissolution.

A Cl-accelerated mechanism, which leads to kinetic Equation 17, had been developed previously for iron [9],

$$X(H_2O) + Cl^- = XOHCl^-_{ads} + H^+ + e \tag{19}$$

$$XOHCl^-_{ads} \xrightarrow{\text{r.d.s.}} XOHCl + e \tag{20}$$

$$XOHCl + H^+ = X^{2+} + H_2O + Cl^- \tag{21}$$

where X represents iron. It is assumed that Step 20 is the rate determining step (r.d.s.) and surface coverage of $XOHCl^-$ ranges between 0.2 and 0.8 so that the surface intermediate follows Temkin

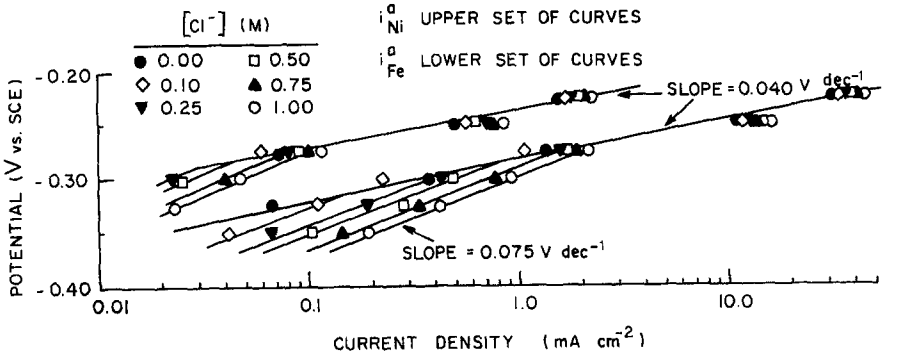

Fig. 8. Effect of Cl^- on electrodissolution rates of iron and nickel components in 1 M ($HCl + HClO_4$).

adsorption behaviour. This mechanism was also applicable to pure nickel in acidic chloride solutions [18].

In Equations 19 to 21, X refers to either iron or nickel for the Fe–5Ni alloy, and the intermediates $FeOHCl^-$ and $NiOHCl^-_{ads}$ are assumed to follow Temkin adsorption behaviour where $0.2 < (\theta_{FeOHCl^-} + \theta_{NiOHCl^-}) < 0.8$. The relative surface coverage θ of each intermediate is assumed to be proportional to the surface concentration of the metal component (alloy electrodissolution in the two Tafel regions is non-selective).

Following the analysis of Gileadi and Conway [28], the rate of the r.d.s. (Equation 20) can be written as

$$r_b = k_b[Cl^-]^{\gamma_b}[H^+]^{-\gamma_b} \exp(\beta_b + \gamma_b)FE/RT \tag{22}$$

If the charge-transfer (β_b) and the adsorption (γ_b) symmetry factors are assumed to be 0.5.

$$r_b = k_b[Cl^-]^{0.5}[H^+]^{-0.5} \exp(FE/RT)$$

Thus, the kinetic equations for the Cl-accelerated mechanism for both iron and nickel components of the Fe–5Ni alloy can be expressed as

$$i^a_{j,Cl} = 2Fk^a_{j,Cl}[Cl^-]^{0.5}[H^+]^{-0.5} \exp(FE/RT) \tag{23}$$

Equation 23 is in good agreement with the empirical relationship for Region A, Equation 17.

The alloy electrodissolution rate of the dominant reaction in Region (A) can be expressed as,

$$i^a(A) = i^a_{Fe}(A) + i^a_{Ni}(A) \tag{24}$$

The individual rates of the metal components, $i^a_{Fe}(A)$ and $i^a_{Ni}(A)$, are given by Equation 17. Since the total rate of alloy electrodissolution in the two Tafel regions is

$$i^a = i^a(A) + i^a(B), \tag{25}$$

where $i^a(B)$ is the rate of the dominant reaction in Region (B),

$$i^a(A) \gg i^a(B)$$

and

$$i^a \approx i^a(A) \tag{26}$$

in Region (A).

The well-known Bockris or OH^- accelerated mechanism [2, 4] leads to kinetic Equation 18,

$$X(H_2O) = XOH_{ads} + H^+ + e \tag{19'}$$

$$XOH_{ads} \xrightarrow{r.d.s.} XOH^+ + e \tag{20'}$$

$$XOH^+ + H^+ = X^{2+} + H_2O \tag{21'}$$

where X represents iron, step 20′ is assumed to be the rate determining step and $\theta_{FeOH} \to 0$ so that FeOH follows Langmuir adsoption behaviour. The results of this study show that the Bockris mechanism is also applicable to the nickel component as well as iron.

In Equations 19′ to 21′, X refers to either iron or nickel for alloy electrodissolution in the higher polarization Region (B), and

$$\theta_{NiOH} < \theta_{FeOH} < \theta_T \to 0$$

where θ_T is the total coverage of all surface intermediates including $FeOHCl^-$ and $NiOHCl^-$. The surface coverages of the latter two,

$$(\theta_{FeOHCl^-} + \theta_{NiOHCl^-}) < \theta_{NiOH}$$

The rate of the r.d.s. (Equation 20′) can be written as

$$r_{b'} = k_{b'}[H^+]^{-1} \exp(1 + \beta_{b'})FE/RT \tag{27}$$

If the symmetry factor ($\beta_{b'}$) is assumed to be 0.5,

$$r_{b'} = k_{b'}[H^+]^{-1} \exp(3FE/2RT)$$

Thus, the kinetic equations for the OH-accelerated mechanism for both iron and nickel components of the Fe–Ni alloy can be expressed as

$$I^a_{j,OH} = 2Fk^a_{j,OH}[H^+]^{-1} \exp(3FE/2RT) \tag{28}$$

Equation 28 is in accord with the empirical kinetic expression for Region B, Equation 18.

In Region (B) then,

$$i^a(B) \gg i^a(A)$$

and

$$i^a \approx i^a(B) \tag{29}$$

where

$$i^a(B) = i^a_{Fe}(B) + i^a_{Ni}(B) \tag{30}$$

Equation 18 gives the individual rate expressions for $i^a_{Fe}(B)$ and $i^a_{Ni}(B)$.

5. Conclusions

Anodic polarization of Fe–5Ni alloy in deoxygenated acid chloride solutions (1 M ionic strength) and atomic absorption spectrophotometry analysis of the solutions to determine steady state dissolution rates of the iron and nickel components were measured. The rates of alloy and iron and nickel component dissolution indicate two separate Tafel regions at low polarization (anodic Tafel slope of $0.075\,V\,dec^{-1}$) and at higher polarization (anodic Tafel slope of $0.04\,V\,dec^{-1}$). Electrodissolution was determined to be non-selective in the two Tafel regions. The electrodissolution kinetics of both iron and nickel components follow the Cl-accelerated mechanism in the lower polarization region and the Bockris mechanism in the higher polarization region.

Acknowledgement

This work is part of the University of California Water Resources Center's Saline Water Conversion Program.

References

[1] K. J. Bonhoeffer and K. E. Heusler, *Z. Elektrochem.* **61** (1957) 122.
[2] J. O'M. Bockris, D. Drazic and A. R. Despic, *Electrochim. Acta* **4** (1961) 325.
[3] J. O'M. Bockris and D. Drazic, *ibid.* **7** (1962) 293.
[4] E. J. Kelly, *J. Electrochem. Soc.* **112** (1965) 124.
[5] J. J. Podesta and A. J. Arvia, *Corr. Sci.* **8** (1968) 203.
[6] E. McCafferty and N. Hackerman, *J. Electrochem. Soc.* **119** (1972) 999.
[7] W. J. Lorenz, *Corr. Sci.* **5** (1965) 121
[8] N. A. Darwish, F. Hilbert, W. J. Lorenz and H. Rosswag, *Electrochim. Acta* **18** (1973) 421.
[9] R. J. Chin and K. Nobe, *J. Electrochem. Soc.* **119** (1972) 1457.
[10] H. C. Kuo and K. Nobe, *ibid.* **125** (1978) 853.
[11] N. Sato and G. Okamoto, *ibid.* **111** (1964) 897.
[12] N. Y. Bune, *Protect. Met.* **3** (1967) 36.
[13] K. E. Heusler and L. Gaiser, *Electrochim. Acta* **13** (1968) 59.
[14] R. Piatti and A. J. Arvia, *ibid.* **14** (1969) 541.
[15] M. L. Kronenberg, J. C. Banter, E. Yeager and F. Hovorka, *J. Electrochem. Soc.* **110** (1963) 1007.
[16] M. Turner, G. Thompson and P. A. Brook, *Corr. Sci.* **13** (1973) 985.
[17] G. T. Burnstein and G. A. Wright, *Electrochim. Acta* **20** (1975) 95.
[18] A. Bengali and K. Nobe, *J. Electrochem. Soc.* **126** (1979) 1118.
[19] N. L. Nguyen and K. Nobe, *ibid.* **128** (1981) 1932.
[20] K. Shiobara, Y. Sawada and S. Morioka, *Trans. Jpn. Inst. Met.* **5** (1965) 97.
[21] G. Economy, R. Speiser, F. H. Beck and M. G. Fontana, *J. Electrochem. Soc.* **108** (1961) 337.
[22] R. R. Sayano and K. Nobe, *Corrosion* **25** (1969) 260.
[23] M. Mogensen, G. Bech-Nielsen and E. Maahn, *Proc. 8th Scand. Corr. Congress*, (1978) 81.
[24] H. C. Kuo, Dissertation, UCLA, February 1975.
[25] H. Nord and G. Bech-Nielsen, *Electrochim. Acta* **16** (1971) 849.
[26] G. Bech-Nielsen, *ibid.* **21** (1976) 627.
[27] G. Bech-Nielsen, *ibid.* **27** (1982) 1321.
[28] E. Gileadi and B. E. Conway, 'Modern Aspects of Electrochemistry', Vol. 3 (edited by J. O'M. Bockris and B. E. Conway) Butterworths, London (1984).